Unusual Properties of Hydrogen-Bonded Ferroelectrics: The Case of Cobalt Formate

P. S. Ghosh,[1,2,*] D. DeTellem,[1] J. Ren,[3] S. Witanachchi,[1] S. Ma,[3] S. Lisenkov,[1] and I. Ponomareva[1]
[1]Department of Physics, University of South Florida, Tampa, Florida 33620, USA
[2]Glass & Advanced Materials Division, Bhabha Atomic Research Centre, Mumbai 400 085, India
[3]Department of Chemistry, University of North Texas, CHEM 305D, 1508 W Mulberry Street, Denton, Texas 76201, USA

(Received 24 May 2021; revised 18 November 2021; accepted 21 January 2022; published 18 February 2022)

Hybrid organic-inorganic perovskites is a class of materials with diverse chemically tunable properties and outstanding potential for multifunctionality. We use first-principles simulations to predict room temperature ferroelectricity in a representative of the formate family, $[NH_2NH_3][Co(HCOO)_3]$. The ferroelectricity arises as a "by-product" of structural transition driven by the stabilization of the hydrogen bond. As a consequence the coupling with the electric field is relatively weak giving origin to large intrinsic coercive fields and making material immune to the depolarizing fields known for its detrimental role in nanoscale ferroelectrics. Insensitivity to the electric field and the intrinsic dynamics of the order-disorder transition in such material leads to the supercoercivity defined as significant increase in the coercive field with frequency. Room temperature polarization measurements provide further support for the predictions.

DOI: 10.1103/PhysRevLett.128.077601

Hybrid organic-inorganic perovskites (HOIPs) are a versatile subclass of ABX_3 materials with many desirable properties such magnetism, ferroelectricity, ferroelasticity, and multiferroicity [1]. The topological similarity with conventional inorganic ABX_3 oxide perovskites and the compositional flexibility to accommodate diverse organic or inorganic components, make these materials a perfect playground for exploring new multifunctional properties, like the coexistence of ferroelectricity and magnetism, i.e., multiferroicity [2]. Low synthesis temperature, flexibility, lack of toxic elements—all make them very attractive for the replacement of some of the inorganic functional perovskites. For example, to date the best piezoelectrics and ferroelectrics are inorganic and often contain lead. They are sought to be replaced. While quite a few HOIPs have been reported to exhibit ferroelectricity and piezoelectricity, their spontaneous polarization and Curie temperatures are typically low [3]. The best materials exhibit high Curie temperature but still low polarization [4,5]. Among different HOIPs, hybrid formate perovskites, e.g., $A[M(HCOO)_3]$ with M = Mn, Fe, Co, Ni, Zn, Mg, are very attractive as the formate group linker on the X site opens up the space to accommodate much larger varieties of organic A-site cations, e.g., $(CH_3)_2NH_2$, NH_3NH_2 [6,7]. Several ferroelectric or antiferroelectric formates have been reported [8]. The structural transitions leading to ferroelectricity in these materials is of order-disorder type due to the disorder of the cation [1]. The ordering of the cation stabilizes hydrogen bonding and could give rise to spontaneous polarization [1,6]. Their typical polarization is $\approx 1\ \mu C/cm^2$ and Curie temperature is in the range of 150–200 K [3]. A few exceptions are $[CH_3NH_2NH_2]\times[M(HCOO)_3]$ with M = Mn, Mg, Fe, and Zn [9–11] that undergo phase transition into a polar phase above room temperature.

In this work we combine theoretical and experimental investigations (i) to predict room temperature ferroelectricity in the recently synthesized $[NH_2NH_3][Co(HCOO)_3]$ [12]; (ii) to predict the unusual intrinsic features of such hydrogen-bonded ferroelectric, namely, supercoercivity and immunity to the depolarization effects; (iii) and to propose a first-principles-based methodology to predict electric properties of order-disorder HOIP ferroelectrics.

All the electronic structure calculations were performed using a plane wave based spin-polarized density functional theory (DFT) as implemented in Vienna *ab initio* simulation package (VASP) [13,14]. Electron-ion interactions were described by projector augmented wave (PAW) potentials [15] and generalized gradient approximation (GGA) with Perdew-Burke-Ernzerhof (PBE) parameterization [16] was used for the exchange-correlation part. A Monkhorst-Pack [17] k-space mesh of $5\times5\times3$ in reciprocal space was used for the Brillouin zone integration. The plane wave cutoff energy (E_{cut}) of 700 eV for the basis set was used throughout the simulation. The van der Waals interactions were incorporated within the GGA using the zero damping DFT-D3 method of Grimme *et al.* [18]. The Hubbard U correction was also introduced to take care of the Coulomb repulsion between the localized d electrons of Co, using the method proposed by Dudarev *et al.* [19]. We used $U_{eff} = 2.0$ eV as proposed in previous studies [20,21]. Full structural relaxation (ionic positions and lattice vectors) had been carried out using conjugate gradient algorithm until the residual forces and stress were less than 0.005 eV/Å and 0.01 GPa, respectively. The unit cell was subjected to full structural relaxation using GGA,

GGA + D3, GGA + U, and GGA + U + D3 approaches. Structures used in computations are provided in Ref [22].

Experimentally, $[NH_2NH_3][Co(HCOO)_3]$ was synthesized by mild solution method. To promote solvent diffusion, $Co(NO_3)$ $2.6H_2O$ (1.0 mmol, 0.291 g) in 5.0 mL methanol solution was layered onto 5.0 mL methanol with 95% (78 mmol, 3.2 mL) formic acid and 98% (6.2 mmol, 0.6 mL) hydrazine monohydrate. After 24 h, magenta-colored large rectangular crystals emerged. The rectangular crystals were isolated from the bulk phase and washed with reagent grade ethanol after the mother solvent was removed. Single crystal x-ray diffraction measurements were applied to validate the perovskite structure.

For the polarization measurements the $[NH_2NH_3] \times [Co(HCOO)_3]$ crystals were embedded into polyvinylpyrodine fluoride (PVDF). It is a ferroelectric polymer that exhibits weak piezoelectric properties. PVDF has been used as a binder to form nanocomposites of many inorganic ferroelectrics [23,24]. In the present work, a 2 wt% solution of PVDF was prepared by dissolving 2 g PVDF in 100 mL of N-N dimethylformamide which was used as the ferroelectric binder. The composite was prepared by mixing 0.05 g of the crushed $[NH_2NH_3][Co(HCOO)_3]$ crystals with 1 mL of the PVDF solution, and sonicated for 2 h. Films for measurements were prepared by drop casting 10 mL of the crystal solution top of ITO coated borosilicate glass and drying in air at room temperature. Multiple silver contacts of 0.2 mm diameter were made on the films as the top contacts for the electrical measurements. Polarization measurements were performed at room temperature using a commercial Precision LC Ferroelectric tester with a Trek 609D-6 High Voltage Amplifier, equipped with a probe station. ITO was used as the bottom contact. A bipolar input profile of 58.8 Hz was applied while varying the driving voltage from 25 V to 200 V. The contact area was determined via scanning electron microscopy (SEM) (JEOLJSM-6390LVK). Repeatability of the values was confirmed by using multiple contacts on the same sample and by checking again on a second sample prepared in the same manner.

Experimentally the $[NH_2NH_3][Co(HCOO)_3]$ undergoes structural phase transition from nonpolar (Pnma) to polar ($Pna2_1$) phase around 343 K [12]. The high temperature high symmetry phase is associated with the dynamical disorder of the cation similar to the other members of this family [7,10,25]. The structure obtained by *in situ* single crystal x-ray diffraction analysis at 100 K was used to compute the ground state of $[NH_2NH_3][Co(HCOO)_3]$ [22]. We have considered ferromagnetic (FM) and antiferromagnetic configurations for Co ions (*A*-, *C*-, and *G*-type AFM) as shown in Fig. 1(f). The *G*-AFM configuration is found to be most stable irrespective of adopted computational methodology as evident from Fig. 1(e) which reports relative cohesive energies. Note, that the energy difference between different magnetic configurations is under 0.016 eV/f.u., which suggests their energetic competitiveness and, also, the

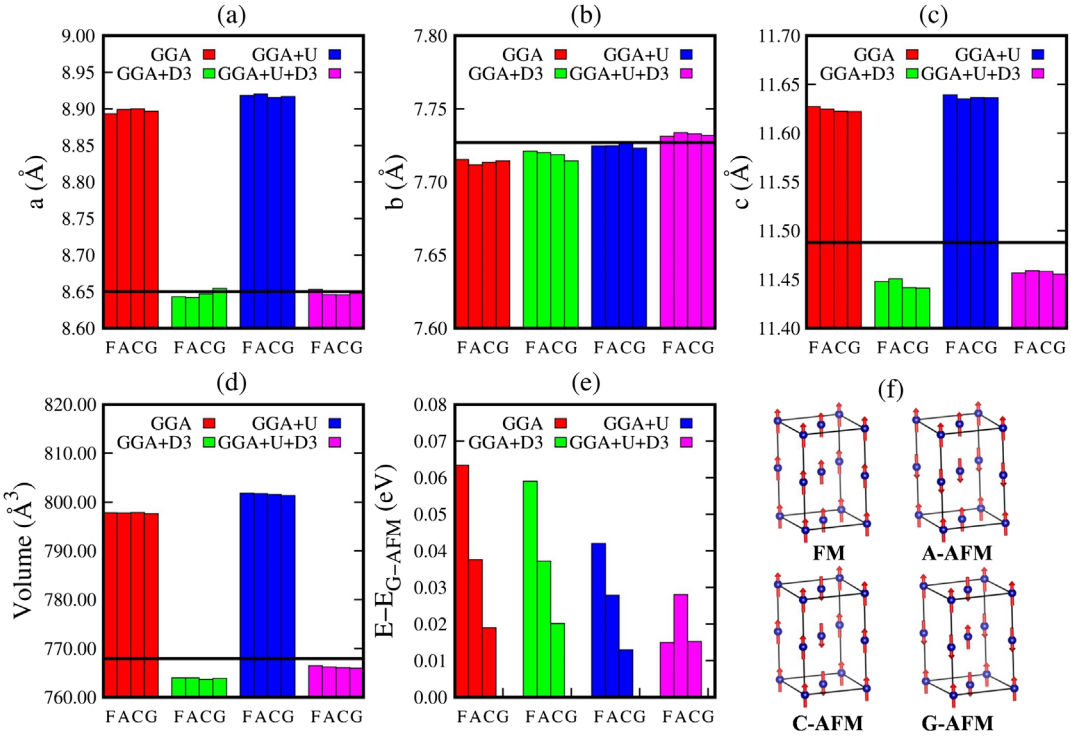

FIG. 1. Lattice parameters (a)–(c), volume (d), and energy gain with respect to *G*-AFM for different magnetic configurations and computational approaches (e). Horizontal lines give experimental values at 100 K [12]. Schematics of magnetic configurations considered in the work (f).

possibility to induce FM ordering by magnetic field. Figures 1(a)–1(d) compare structural parameters obtained with different computational approaches with experimental data. We find that GGA + U + D3 provides the best overall agreement with experiment and, therefore, will be used for the rest of the presentation. The computations predict the magnetic moment on the Co^{2+} is 2.69 μ_B. Interestingly, we notice a slight difference between the structural parameters [see Figs. 1(a)–1(d)] for different types of magnetic ordering which suggests weak magnetostructural coupling.

To compute the polarization in this material from first-principles we construct the roto-distortion path associated with the polarization reversal following the approach suggested in Ref. [26]. Note, that the path includes rotation of the $[NH_2NH_3]^+$ molecule and distortion of the $Co(HCOO)_3$ framework [as shown in Figs. 2(a)–2(b)]. Technically, the experimental high temperature (353 K) phase (HTP) that is associated with the disorder of the $[NH_2NH_3]^+$ is decomposed into two structures, both having $Pna2_1$ space group. Next the roto-distortion path is constructed between these two structures [see Fig. 2(b)] and polarization is computed along the path [see Fig. 2(c)]. The predicted value is 1.81 $\mu C/cm^2$ (along c axis). We have also computed polarization for the experimental low temperature phase (LTP), that is 100 K, [see Fig. 2(c)] and found the value of 2.41 $\mu C/cm^2$. The ground state polarization is 2.56 $\mu C/cm^2$ which is comparable with experimental measurements (2.6–3.6 $\mu C/cm^2$) on similar materials [7]. We expect at finite temperatures the polarization to range between 1.81 and 2.56 $\mu C/cm^2$. Analysis of HTP phase and the ground state reveals that structural phase transition is associated with ordering of $[NH_2NH_3]^+$ driven primarily by the stabilization of the H bond. In both phases there are five H bonds per $[NH_2NH_3]^+$ molecule, the length of bond ranging from 1.7 to 2.5 Å [27]. The average length of the H bond decreases by 3% in the ground state. Note, that hydrogen-bonding strengths of formate perovskites range from 0.36 to 1.40 eV/cation [27].

The energy evolution along the polarization reversal path in both the LTP and HTP phase is given in Fig. 2(d). Both phases exhibit two degenerate energy minima associated with the opposite polarization direction, however, in the HTP the minima are significantly shallower suggesting the possibility of hopping between them at finite temperatures. The presence of the two minima above the T_C differentiates this material from the inorganic ferroelectric perovskites,

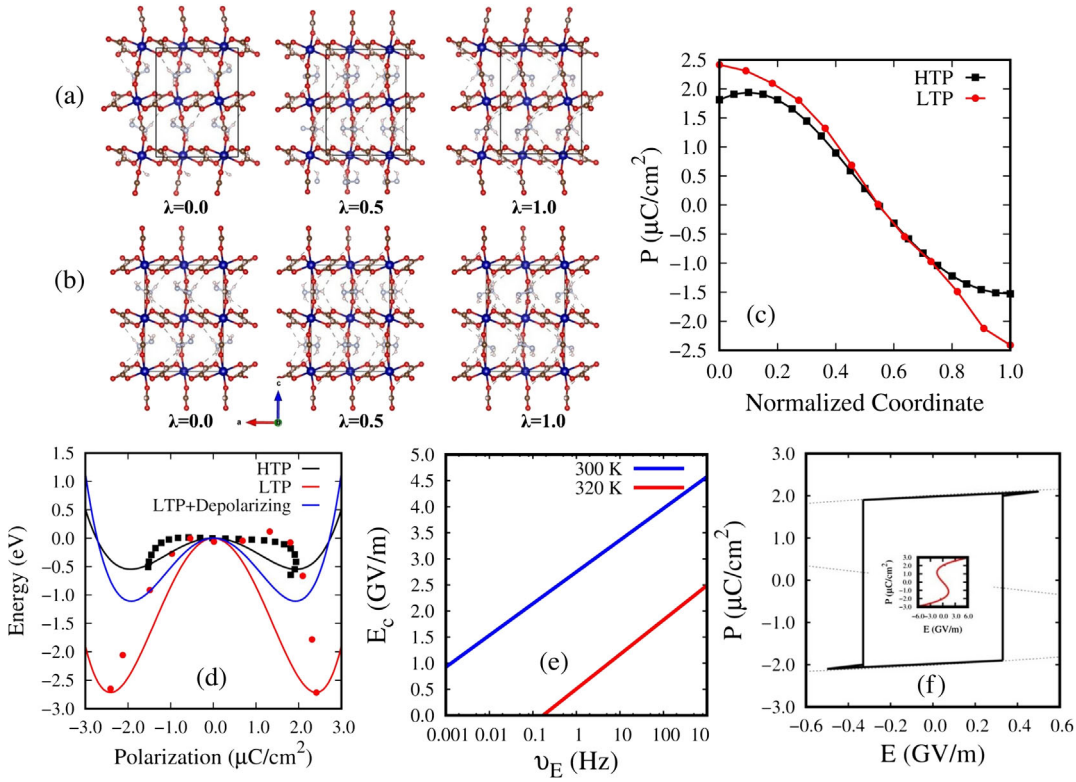

FIG. 2. Roto-distortion path [presented as normalized coordinate (λ)] of LTP (a) and HTP (b). Color scheme: Co, blue; O, red; C, brown; N, light blue; H, gray. The end points of the path, $\lambda = 0$ and 1, correspond to the phase and its inversion. Polarization along the roto-distortion path for LTP and HTP (c). Energy as a function of polarization along the roto-distortion path for different phases (d). Points represent computational data while solid lines give fit by the fourth order polynomial as described in the text. LTP + depolarizing indicates the LTP with the addition of the depolarizing field contribution; the dependence of the coercive field on the frequency of the applied electric field (e); hysteresis loop computed at 300 K (f). Inset gives the $P(E)$ associated with the equation of state.

whose high temperature phase is typically associated with a single minima at $P = 0$. It is possible that the presence of the two minima originates from lower symmetry of the organic molecule. The hopping between the minima is also characteristic of order-disorder phase transitions.

To estimate the hopping rates between the two minima we use transition state theory within the framework of "Bennet-Chandler" approach [28]. The model predicts the barrier crossing rate, $k_{\mathrm{hop}} = \frac{1}{2}|\dot{q}|[(e^{-\beta U(q^*)})/(\int_{\infty}^{q^*} dq e^{-\beta U(q)})]$, where q is the dipole moment of the formula unit, $\beta = [1/(k_B T)]$, and q^* is the location of the energy barrier. We follow the derivations of Ref. [29] to obtain $k_{\mathrm{hop}} \approx \nu e^{-\beta \Delta U}$, where ΔU is the height of the barrier and $\nu = [(\prod_{i=1}^{N} \nu_i)/(\prod_{k=1}^{N-1} \nu_k^{\dagger})]$ is the "effective" vibrational frequency of the $[NH_2NH_3]^+$ molecule in the minimum. In the latter expression ν_i is the frequency of the ith normal mode of the molecule in the energy minimum, while $\nu_k^{\dagger}$ is the kth normal mode of the molecule at the transition state (energy maximum), N is the number of normal modes for the molecule in the energy minimum. Note, that at the transition state, one of the normal mode's frequencies is imaginary so the product includes only $N - 1$ terms. It is established that the hopping rate is rather insensitive to prefactor ν, so the common practice is to use simple estimates of 1–10 THz [29]. To ensure that such estimates are valid in our case we computed the $[NH_2NH_3]^+$ frequencies and found them to be in the range of 3.7–100 THz in agreement with experimental data [30]. Technically the frequencies were computed by diagonalizing the block of the dynamical matrix associated with the molecule [29]. As in our model polarization reversal originates from mostly rigid rotation of the $[NH_2NH_3]^+$, the "effective" frequency of the normal mode polarized along the rotation path is at the lowest end of the spectrum. These considerations suggest using $\nu = 1$ THz for the prefactor in the k_{hop} expression. Following the Landau theory of phase transitions we interpolate DFT energies with fourth order polynomial [see Fig. 2(d)] $U(P) = U_{\mathrm{min}}[2(P/P_{\mathrm{min}})^2 - (P/P_{\mathrm{min}})^4]$, where U_{min} and P_{min} are the energy and polarization values in the minima. Note that the hopping rate is only sensitive to the height of the energy barrier and not the fit. The application of this approach to obtain hopping rates for the LTP and HTP phases yielded of 0.0 s^{-1} and 1.6×10^4 s^{-1}, respectively. The rates predict ferroelectric and paraelectric phases at 100 and 353 K, respectively. Since at room temperature the structure is in the $Pna2_1$ space group we used the LTP energy profile to estimate room temperature hopping rates and found that rate to be 0.0 s^{-1}, which predicts the ferroelectric phase. This prediction has been further validated through computations on room temperature structure from experiment.

Next we extend the order-disorder model to the case when the material is subjected to electrical field, E, and write the enthalpy as $H(P, E) = U(P) - PEV$, where V is the supercell volume. The electric field term removes the energy degeneracy for the $\pm P_{\mathrm{min}}$ shifting one of the minima up while another one down. The former one becomes the metastable phase, while the latter one is the stable one. The hopping rates between the two minima can now be approximated as $k_{\mathrm{hop}}(E) \approx \nu e^{-\beta(\Delta U + PEV)}$. At the coercive field, E_c, the sample undergoes transition from the metastable to the stable phases. If the applied field is an ac field with frequency ν_E then for the transition to occur $\nu_E \approx 2k_{\mathrm{hop}} \approx 2\nu e^{-\beta(\Delta U - |P|EV)}$. Conceptually, the field lowers barrier for the metastable phase and, therefore, increases the hopping rates as compared to the field-free case. Note that the factor of 2 in front of the k_{hop} is because during one cycle of the field the system has to complete two hops between the metastable and stable phases. For the transition to occur for the given ν_E the field has to increase until the hopping rates become comparable with the electric field frequency. The smallest field to allow for the transition is the coercive field and can be estimated as $E_c = [\Delta U - k_B T \ln(2\nu/\nu_E)]/|P|V$. The expression predicts that in agreement with experiment [31] the coercive field exhibits frequency dependence, that is, it increases with the frequency [31]. To incorporate temperature dependence into ΔU we recall that within the Landau theory of phase transitions some coefficients of the energy expansion $U(P)$ are taken to be linearly dependent on temperature. In this spirit we assume linear dependence on temperature for both P_{min} and U_{min} and fit it to the HTP and LTP values. Figure 2(e) shows the dependence of the coercive field on the frequency for two temperatures, 300 and 320 K. There are three features to note from the data. The first one is that below a certain frequency the coercive field could become zero which means that the frequency is lower than the intrinsic hopping rate and the material may appear as paraelectric. Second, if the applied field is lower than the coercive field for a given temperature the ferroelectric loops cannot occur (or will be highly distorted). Indeed it was observed experimentally, that below 40 kV/cm no hysteresis loops occur [31]. We can also see that increase in frequencies causes an increase in the coercive field, that is supercoercivity, reported experimentally [31]. Third, the intrinsic coercive field is very large. The origin of this can be traced to the fact that ferroelectricity is induced by the structural transition due to H-bond stabilization rather than the dipole-dipole interaction as in inorganic displacive ferroelectrics. Consequently, the net dipole moment comes as a bonus but is rather small. As a result the energy contribution due to interaction with the applied electric field is small in comparison with the barrier due to H-bond breakage so that the applied field has to be really large to switch the direction of polarization. Such supercoercivity is likely to be a general feature of the hybrid organic-inorganic ferroelectrics whose polarization arises from structural phase transition due to H-bond stabilization.

Interestingly, such "insensitivity" to the applied field suggests that the material may exhibit similar insensitivity to the depolarizing field that is inherent to ferroelectric nano-structures. The depolarizing field arises due to the presence of uncompensated surface charge and is detrimental to the ferroelectricity of nanostructures [32–34]. In fact, the depolarizing field is the sole reason for ferroelectricity disappearance at the nanoscale in inorganic perovskites. To explore the role of the depolarizing field in hybrid ferroelectrics we augment $U(P)$ with the depolarizing energy term $2\pi P^2 V/\varepsilon_0$ associated with two-dimensional, or thin film, geometry. The resulting LTP energy is plotted in Fig. 2(d) and demonstrates the presence of two minima even in the absence of any surface charge screening. The addition of depolarizing energy renormalizes the polarization and energy in the minima as follows: $P_{\min}^{\mathrm{dep}} = P_{\min}(\sqrt{1+a})$ and $U_{\min}^{\mathrm{dep}} = U_{\min}(1+a)^2$, where $a = \pi P_{\min}^2 V/\varepsilon_0 U_{\min}$. Application of our model to the renormalized energy profile predicts a zero hopping rate, that is the ferroelectric phase, at 100 K even in the presence of fully unscreened depolarizing field. On the other hand, in the absence of surface charge screening their inorganic counterparts lose net polarization [35] along the direction associated with the depolarizing field. It should be noted that both unusual properties, supercoercivity and immunity to the depolarizing field, revealed here are the intrinsic effects. The extrinsic effects that will contribute in measurements include polarization reversal via domain formation and propagation, which will lower the coercive field. The depolarizing field could be at least partially compensated by the surface charge screening (due to either presence of the sample defects or the surface adsorbates) which will further stabilize the ferroelectricity in nanostructures.

Finally, we extend our approach to predict finite-temperature intrinsic hysteresis loops from first-principles calculations. We first plot $P(E)$ from the interpolated dependence $H(P,E,T)$ following the approach of Ref. [26]. In particular, we obtain the equation of state from $(\partial H/\partial P)_{E,T} = 0$ which yields $P(E)$ given in the inset to Fig. 2(f). Next $E_c(T,\nu_E)$ is computed from our model and used to connect metastable and stable phases as shown in Fig. 2(f) for $\nu_E = 10$ Hz at room temperature. Of course, inclusion of the depolarizing field will further decrease the coercive field [36].

To verify some of the predictions experimentally we have measured the dependence of the polarization on the electric field for the $[NH_2NH_3][Co(HCOO)_3]$ films embedded in PVDF under different electric field amplitude and frequencies. In particular, the amplitudes ranged from 5 to 34.5 kV/cm while the frequency varied in the range of 0.125 to 1000 Hz. Figure 3 shows one representative dependence for the largest electric field that we were able to apply to the sample and compares it with that of pure PVDF. Indeed, in agreement with our computational predictions as well as Ref. [31] no hysteresis loops were observed for this field. The finding provides experimental support for our computational prediction of a large intrinsic coercive field. As a note, no significant dependence on the frequency in the low field regime was found.

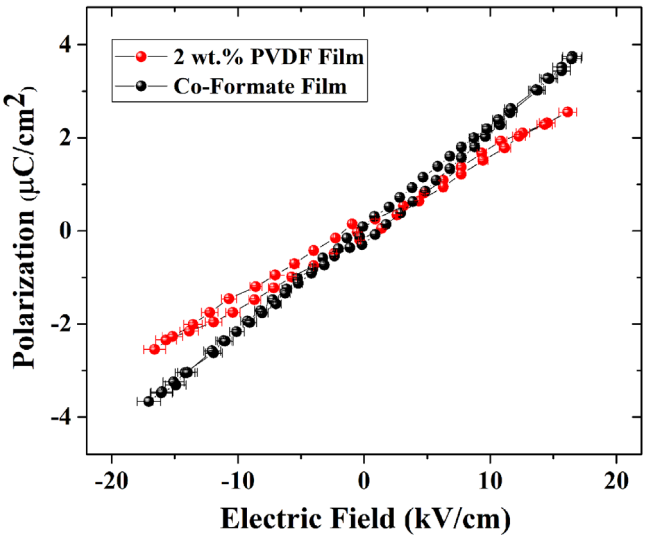

FIG. 3. Room-temperature polarization in drop-casted $[NH_2NH_3][Co(HCOO)_3]$ film and drop-casted 2% PVDF film recorded at 58.8 Hz.

In summary, we investigated ferroelectricity in $[NH_2NH_3][Co(HCOO)_3]$ HOIP using a combined computational and experimental approach. We predicted the room temperature ferroelectricity in this material which is rare among the formate family. The ground state polarization was found to be 2.56 $\mu C/cm^2$. The ferroelectricity in this material is due to alignment of $[NH_2NH_3]^+$ molecules and occurs as a bonus from the structural phase transition driven by the H-bond stabilization. Consequently, the material exhibits relatively weak coupling with the electric field which leads to the large intrinsic coercive field and supercoercivity. The other consequence of the weak coupling to the electric field is the immunity to the depolarizing field. Such field is known to be detrimental to the nanoscale ferroelectricity in inorganic ferroelectrics. The first-principles model is developed to predict the dynamics of the order-disorder phase transition in such materials. The model is capable of predicting the dependence of the intrinsic coercive field on the applied field frequency and of ferroelectric hysteresis loops.

This work is supported by the National Science Foundation under the grant EPMD-2029800.

*psghosh@mail.usf.edu

[1] W. Li, Z. Wang, F. Deschler, S. Gao, R. H. Friend, and A. K. Cheetham, Nat. Rev. Mater. **2**, 16099 (2017).
[2] B. Saparov and D. B. Mitzi, Chem. Rev. **116**, 4558 (2016).

[3] K. Asadi and M. A. van der Veen, Eur. J. Inorg. Chem. **2016**, 4332 (2016).
[4] Y. You, W. Liao, D. Zhao, H. Ye, Y. Zhang, Q. Zhou, X. Niu, J. Wang, P. Li, D. Fu, Z. Wang, S. Gao, K. Yang, J. Liu, J. Li, Y. Yan, and R. Xiong, Science **357**, 306 (2017).
[5] W. Liao, D. Zhao, Y. Tang, Y. Zhang, P. Li, P. Shi, X. Chen, Y. You, and R. Xiong, Science **363**, 1206 (2019).
[6] P. Jain, V. Ramachandran, R. Clark, H. D. Zhou, B. Toby, N. Dalal, H. Kroto, and A. Cheetham, J. Am. Chem. Soc. **131**, 13625 (2009).
[7] S. Chen, R. Shang, K.-L. Hu, Z.-M. Wang, and S. Gao, Inorg. Chem. Front. **1**, 83 (2014).
[8] Y. Ma and Y. Sun, J. App. Phys. **127**, 080901 (2020).
[9] M. Maczka, A. Gagor, M. Ptak, W. Paraguassu, T. A. da Silva, A. Sieradzki, and A. Pikul, Chem. Mater. **29**, 2264 (2017).
[10] A. Sieradzki, M. Maczka, M. Simenas, J. K. Zareba, A. Gagor, S. Balciunas, M. Kinka, A. Ciupa, M. Nyk, V. Samulionis, J. Banys, M. Paluch, and S. Pawlus, J. Mater. Chem. C **6**, 9420 (2018).
[11] M. Šimėnas, S. Balčiūnas, M. Trzebiatowska, M. Ptak, M. Maczka, G. Völkel, A. Pöppl, and J. Banys, J. Mater. Chem. C **5**, 4526 (2017).
[12] W. D. C. B. Gunatilleke, K. Wei, Z. Niu, L. Wojtas, G. Nolas, and S. Ma, Dalton Trans. **46**, 13342 (2017).
[13] G. Kresse and J. Furthmuller, Comput. Mater. Sci. **6**, 15 (1996).
[14] G. Kresse and J. Furthmüller, Phys. Rev. B **54**, 11169 (1996).
[15] P. E. Blöchl, Phys. Rev. B **50**, 17953 (1994).
[16] J. P. Perdew, K. Burke, and M. Ernzerhof, Phys. Rev. Lett. **77**, 3865 (1996).
[17] H. J. Monkhorst and J. D. Pack, Phys. Rev. B **13**, 5188 (1976).
[18] S. Grimme, J. Antony, S. Ehrlich, and H. Krieg, J. Chem. Phys. **132**, 154104 (2010).
[19] S. L. Dudarev, G. A. Botton, S. Y. Savrasov, C. J. Humphreys, and A. P. Sutton, Phys. Rev. B **57**, 1505 (1998).
[20] V. Fung, F. F. Tao, and D. en Jiang, Chem. Cat. Chem. **10**, 244 (2018).
[21] J. Liu, S. Zhang, Y. Zhou, V. Fung, L. Nguyen, D. Jiang, W. Shen, J. Fan, and F. F. Tao, ACS Catal. **6**, 4218 (2016).
[22] P. S. Ghosh, S. Lisenkov, and I. Ponomareva, NH_2NH_3–$(HCOO)_3$ experimental structure, https://github.com/USFmatscilab/NH2NH3-Co-HCOO_3 (2021).
[23] S. K. Pradhan, A. Kumar, A. N. Sinha, P. Kour, R. Pandey, P. Kumar, and M. Kar, Ferroelectrics **516**, 18 (2017).
[24] M. Panda and A. Trivedi, Ferroelectrics **572**, 246 (2021).
[25] A. Simonov and A. L. Goodwin, Nat. Rev. Chem. **4**, 657 (2020).
[26] M. Kingsland, P. S. Ghosh, S. Lisenkov, and I. Ponomareva, J. Phys. Chem. C **125**, 8794 (2021).
[27] K. L. Svane, A. C. Forse, C. P. Grey, G. Kieslich, A. K. Cheetham, A. Walsh, and K. T. Butler, J. Phys. Chem. Lett. **8**, 6154 (2017).
[28] D. Frenkel and B. Smit, *Understanding Molecular Simulation—From Algorithms to Applications (page 440)* (Academic Press, New York, 1996).
[29] D. Sholland J. Steckel, *Density Functional Theory: A Practical Introduction* (Wiley Press, New York, 2009).
[30] A. Mattioda and R. Frech, Spectrochim. Acta Part A **53**, 1767 (1997).
[31] J. Walker, R. Miranti, S. L. Skjærvø, T. Rojac, T. Grande, and M.-A. Einarsrud, J. Mater. Chem. C **8**, 3206 (2020).
[32] J. Junquera and P. Ghosez, Nature (London) **422**, 506 (2003).
[33] D. D. Fong, G. B. Stephenson, S. K. Streiffer, J. A. Eastman, O. Auciello, P. H. Fuoss, and C. Thompson, Science **304**, 1650 (2004).
[34] E. Glazkova, K. McCash, C.-M. Chang, B. K. Mani, and I. Ponomareva, Appl. Phys. Lett. **104**, 012909 (2014).
[35] I. Ponomareva and L. Bellaiche, Phys. Rev. B **74**, 064102 (2006).
[36] M. Kingsland, Z. G. Fthenakis, and I. Ponomareva, Phys. Rev. B **100**, 024114 (2019).